Synthesis of a predicted layered LiB via cold compression

A. N. Kolmogorov, S. Hajinazar, C. Angyal, V. L. Kuznetsov, and A. P. Jephcoat

Phys. Rev. B **92**, 144110 — Published 29 October 2015

DOI: 10.1103/PhysRevB.92.144110

Synthesis of a predicted layered LiB via cold compression

A.N. Kolmogorov,[1] S. Hajinazar,[1] C. Angyal,[1] V.L. Kuznetsov,[2] and A.P. Jephcoat[3]
[1]*Department of Physics, Applied Physics and Astronomy, Binghamton University, State University of New York, PO Box 6000, Binghamton, New York 13902-6000, USA*
[2]*Department of Chemistry, University of Oxford, South Parks Road, Oxford OX1 3QR, UK and*
[3]*Institute for Study of the Earth's Interior, Okayama University, Misasa, Tottori 682-0193, Japan*
(Dated: October 2, 2015)

We have discovered a stoichiometric LiB with hexagonal boron layers by compressing known $LiB_{0.9}$ with linear boron chains. The *sp* to sp^2 rebonding occurred at *room* temperature and moderate pressures above 21 GPa. The study was motivated by a long-standing prediction that LiB in the stable layered configuration could be a close analog to the MgB_2 superconductor. Apparent stacking disorder in LiB and an evidenced stoichiometry shift in LiB_y (down to $y \approx 0.75$) made the materials' characterization a challenge. *Ab initio* modeling allowed us to establish LiB_y's pressure-dependent composition and predict overlooked related stable structures. The synchrotron powder diffraction data indicates that synthesized LiB remains metastable under ambient pressure.

I. INTRODUCTION

Abundant elements at the top of the periodic table are key ingredients in the design of advanced materials for energy transport and storage. H and B atoms give rise to high-frequency phonon modes that are essential for high critical temperatures (T_c) in phonon-mediated superconductors, such as the proposed metallic H under high pressures[1] or the recently discovered MgB_2 superconductor[2]. Li and H are efficient carriers of (electro)chemical energy that can be packed in non-carbon-based high-capacity systems, e.g., Li-ion batteries[3,4] or Li-B-H hydrogen storage compounds[5].

The challenges of developing such materials for practical applications have been widely discussed[3–6]. In superconductivity, the T_c tends to be inversely correlated with material's thermodynamic stability and is hard to predict from first principles[7–9]. In fact, early confirmed predictions of new superconductors were limited mostly to pressure-induced transitions in known Si and Li elemental systems[10,11]. A recently proposed[12] and discovered[13] FeB_4 compound (meta)stable under ambient conditions in a previously unknown structure is a superconductor designed fully *in silico*. The latest landmark observation of T_c near 200 K at about 90 GPa[14] in a proposed H-S binary material[15] is a striking example of theory-guided discovery that is bound to re-energize the search for new conventional superconductors.

In this study we test another long-standing *ab initio* prediction: a surprisingly simple structure was identified and shown to stabilize under moderate pressures in the binary Li-B system[16,17]. The previously unknown four-atom prototype can be derived from an unusual fcc-type stacking said to be a "Nature's missing structure"[18]. It was shown that the originally close-packed configuration transforms into a "metal sandwich" motif with MgB_2-type hexagonal B layers stabilized by two Li rather than one Mg layers[17]. *Ab initio* studies have revealed important similarities and differences in the superconducting features of MgB_2 and LiB, most notably the long-sought-after higher density of states (DOS) of key p_σ-B states in the latter material[16,17,19–21]. One of the most promising proposed high-T_c superconductors so far, a hole-doped Li_xBC compound[22], did not exhibit superconductivity above 2 K[23]. Synthesis and characterization of LiB with a predicted T_c of $\sim$ 10 K could help establish beneficial factors in the design of MgB_2-type superconductors. Probing the known LiB_y compound's range of stability would also give information on whether it is possible to synthesize such hydrogen-rich derivatives as the proposed metastable $LiBH/LiBH_2$ phases[24].

The particular difficulties for the theoretical stability analysis and the experimental characterization of new LiB-based materials arise from the complexity of the starting $LiB_{y\approx0.9}$. Wörle and Nesper were first to deduce the linear chain morphology of the B network and the apparent incommensurability of the Li and B sublattices based on powder diffraction data[25,26]. Our previous *ab initio* work showed the material to be a unique *adaptive* compound with a finite stability range at *zero* temperature. The results indicated that hydrostatic pressure should stabilize more Li-rich $LiB^{1D}_{y-\delta}$ stoichiometries (the superscript denotes the B framework dimensionality) and that the starting material would not fully convert into LiB^{2D}[17]. For example, compression of $Li_8B^{1D}_7$ could produce nearly equal (1:7/8) amounts of stable LiB^{2D} and $Li_4B^{1D}_3$ phases. The predicted stability of the proposed stoichiometric LiB^{2D} under several GPa pressure has been reproduced in a number of recent *ab initio* studies[27–30]. Yet, a systematic attempt by Lazicki *et al.* to synthesize the material in diamond anvil cells (DACs) reportedly showed no indication of structural transformations in LiB^{1D}_y up to 70 GPa[31].

In the present work we describe DAC experiments which revealed a convoluted dependence of LiB^{1D}_y powder X-ray diffraction (XRD) patterns on pressure and led to appearance of new reflections at *room* temperature and moderate pressures of 21 GPa. By comparing these observations with our density functional theory (DFT) results, we established irreversible pressure-

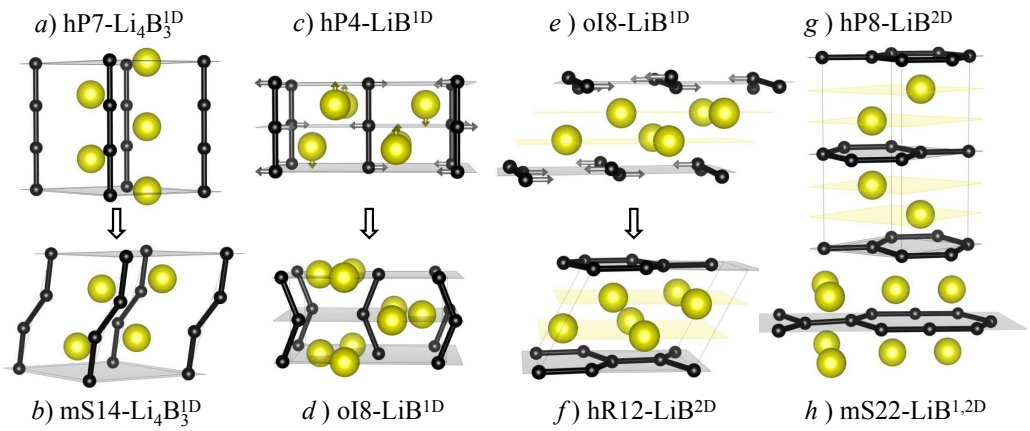

FIG. 1: (color online) Known and predicted Li-B structures denoted with Pearson symbols. The (a)→(b) and (c)→(d) transformations are due to soft-mode instability. (d,e) are different views of oI8-LiB^{1D} showing relationships to other structures. The arrows in (e) show a possible pathway transforming B chains into B layers. (f,g) ABC and AB stackings of the predicted LiB^{2D} material. (h) A metastable structural motif comprised of 1D and 2D units.

induced changes in the LiB_y^{1D} composition and matched a new dominant peak with the signature (002) reflection from the proposed LiB^{2D}. Our data indicates that the compound can be quenched down to 1 bar.

The rest of the paper is organized as follows. The computational and experimental methods are described in Sec. II, the stability analysis and derived relevant phases are discussed in Sec. III, the XRD results are presented and interpreted in Sec. IV, and the conclusions are given in Sec. V.

II. METHODOLOGY

A. Simulation setup

Stability of Li-B compounds was examined at the DFT level with with VASP[32]. The 500 eV energy cutoff and dense k-meshes, $N_{k1} \times N_{k2} \times N_{k3} \times N_{atoms} \geq 4,000$[33], ensure numerical convergence of the formation energy differences to typically within 1-2 meV/atom. We employed projector augmented wave potentials[34] which treats the 1s states of Li as semi-core. All final results were obtained with the Perdew-Burke-Ernzerhof (PBE) exchange-correlation (xc) functional[35] within the generalized gradient approximation (GGA)[36]. Selected calculations were repeated using the Perdew-Zunger parameterization within the local density approximation (LDA)[37] and optB86b parameterization of with the van der Waals corrections[38]. As described in the supplementary material (SM)[39], we showed that systematic errors are considerable but the predicted LiB should become thermodynamically stable by $\sim$ 10 GPa regardless of the exchange-correlation functional choice or the vibrational entropy correction to Gibbs energy at room temperature. The phonons were calculated with the finite displacement method as implemented in PHON[40] and the evolutionary searches for new ground state structures were performed with the MAISE package[41]. The ordered layered LiB was modeled as two possible stackings ABC and AB shown in Fig. 1(f,e) (the latter structure is known as the BaCu prototype[42]). Simulation settings and relevant structures (referred to by their Pearson symbol) are further detailed in SM[39].

B. Synthesis and characterization setups

Our starting material with a nominal composition of $LiB_{0.95}$ was synthesized from pure elements and stored in paraffin oil as explained in SM[39]. X-ray characterization of samples was done at the I15 Beamline at the Diamond Light Source, with the first signs of the (002) peak from the layered LiB observed in 2009. The DAC and X-ray setups[39] were similar to those described in our previous study[43]. The complex behavior of LiB_y^{1D} was studied by using different pressure media (oil, Ar, and H_2) and by examining powder XRD patterns during compression-decompression runs in pressure ranges up to 39 GPa. The particular challenge in these experiments was the broadness and the weakness of the signature peak from the layered phase. The well-resolved signals from the phase at each pressure were obtained after performing multiple 10 to 30-min synchrotron shots across the sample and real-time theoretical analysis of the data. The 2D signals were recorded on a MAR345 image plate and integrated with FIT2D[44,45] software. We used Topas Academic[46] to perform LeBail fitting of the integrated powder XRD signals.

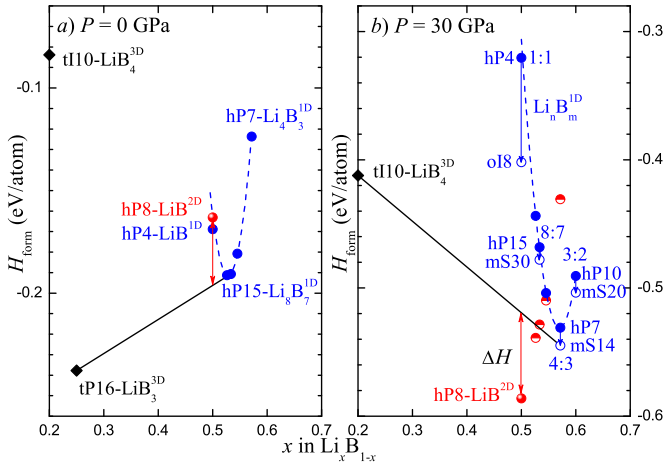

FIG. 2: (color online) Formation enthalpy calculated with DFT at $T = 0$ K. The dashed lines are parabolic fits for the $Li_{2n}B_m^{1D}$ family with linear B chains. The black solid lines show how to calculate relative stability for the predicted hP8-LiB^{2D} in Fig. 3. The hollow blue points correspond to derived structures with distorted 1D B chains. The semi-filled red points denote structures with both 1D and 2D B networks.

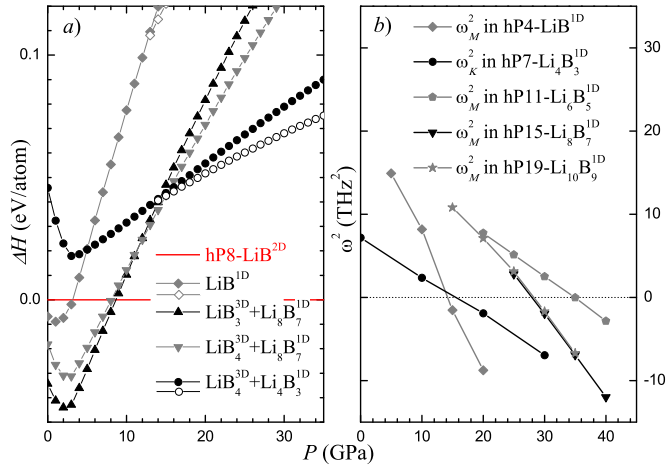

FIG. 3: (color online) (a) Relative stability of hP8-LiB^{2D} calculated with DFT for different combinations of Li-B phases at 0 K. hP8-LiB^{2D} becomes stable at 8.6 GPa. (b) Calculated softening of key phonon modes illustrating pressure-induced destabilization of selected $Li_{2n}B_m^{1D}$ phases.

III. STABILITY ANALYSIS AND PREDICTION OF DERIVED PHASES WITH DFT

We began re-examination of the Li-B compound stability with DFT-based dynamical stability analysis for previously considered phases. Unexpectedly, our frozen phonon calculations[39,40] revealed that the family of $Li_{2n}B_m^{1D}$ phases across a large composition range becomes dynamically unstable under moderate pressures, a behavior not recognized in previous *ab initio* studies[17,27–30,47,48]. Construction of most stable derived structures is a known challenge due to the possibility of multiple local minima with similar energies/enthalpies[43,49,50]. We carefully examined relevant stoichiometries with $1/2 \leq x \leq 4/7$ under relevant (P, T) conditions and identified several dynamically stable derivatives. In addition to following phonon modes with imaginary frequencies we performed evolutionary searches described in SM[39].

A soft-mode phase transition from hP4-LiB^{1D} to oI8-LiB^{1D} [see Fig. 1(c,d), 2(b), S6, S7] was found at $\sim$ 14 GPa. The oI8 structure with zig-zagged B chains metastable in this case was predicted to be thermodynamically stable for the related CaB binary[50]. The instability of hP4-LiB^{1D} has been associated with a large DOS(E_{Fermi}) which can be lowered by change in stoichiometry[17] or the proposed distortion at high pressures (Figs. S8-10). hP7-$Li_4B_3^{1D}$ became dynamically unstable at a similar $\sim$ 15 GPa pressure. A related mS14 phase with snake-like B chains at the 4:3 composition [Fig. 1(b)] was found to be thermodynamically stable at 30 GPa with respect to all phases considered here and in Ref. 30. hP15-$Li_8B_7^{1D}$ developed a phonon mode with an imaginary frequency at much higher $P \sim 28$ GPa and could be transformed into a lower-symmetry mS30 structure. The faster destabilization of the 1:1 and 4:3 $Li_{2n}B_m^{1D}$ phases upon compression is not unexpected, as it is easier for B chains to bend and for the Li atoms to rearrange if the two sublattices have a short common period. Interestingly, our unconstrained search revealed competitive metastable structures comprising unusual combinations of 1D linear chain and 2D hexagonal units [Figs. 1(h)][39]. The observed enthalpy gains shown in Fig. 2(b) are noticeable but not sufficient to destabilize the predicted hP8-LiB^{2D} phase.

This identification of a suite of more stable LiB_y^{1D} $(1.0 \geq y \geq 0.67)$ phases with distorted B chains in the 14-30 GPa range has two important consequences. First, interpretation of XRD patterns may be further compli-

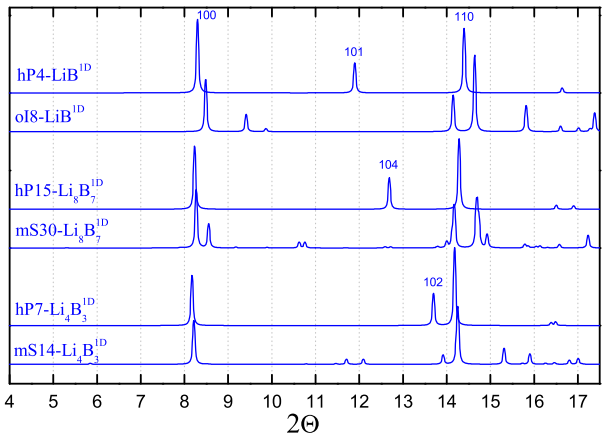

FIG. 4: (color online) Simulated XRD patterns for $Li_{2n}B_m^{1D}$ phases at 30 GPa. The (dynamically unstable) hexagonal structures have straight linear B chains and the proposed (dynamically stable) orthorhombic or monoclinic structures have buckled B chains.

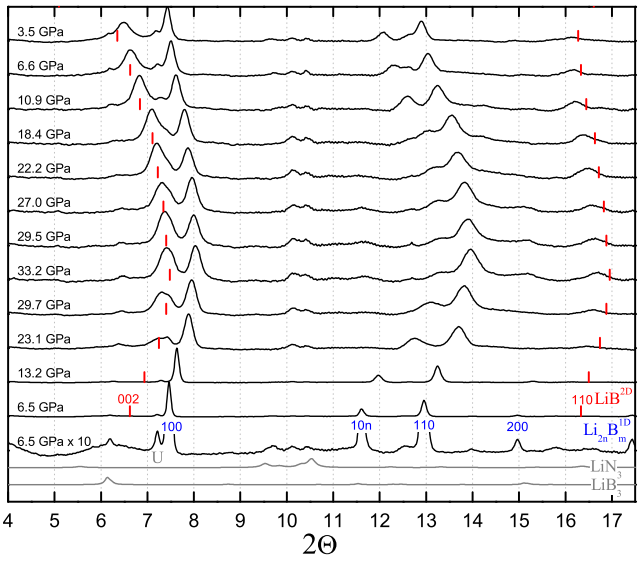

FIG. 5: (color online) Evolution of powder XRD peaks observed for LiB_y in paraffin oil at 6.5 → 33.2 → 3.5 GPa pressures. The red markers indicate key peak positions calculated with DFT for the predicted layered hP8-LiB^{2D} phase. The strong peaks in the magnified pattern at 6.5 GPa correspond to $Li_{2n}B_m^{1D}$ reflections. Some of the weak peaks could be matched with lines in the simulated LiB_3/LiN_3 patterns at $P = 6.5$ GPa. The 7.2 degree peak comes from an unidentified phase.

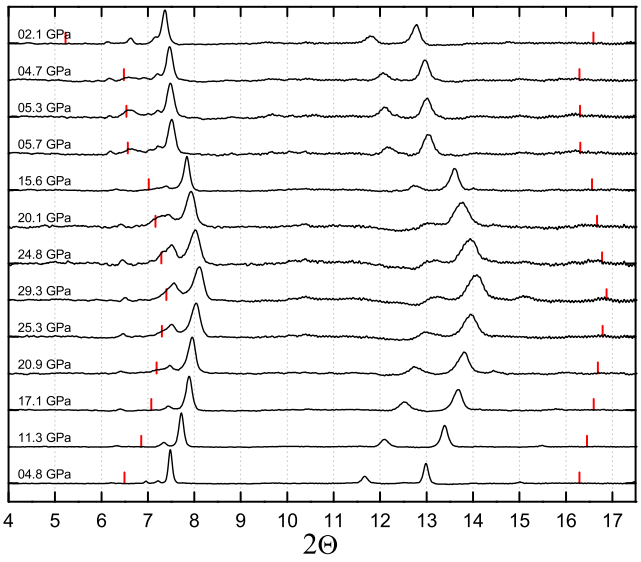

FIG. 6: (color online) Evolution of powder XRD peaks from LiB_y in the H_2 pressure medium at room temperature and 4.8 → 29.3 → 2.1 GPa pressures. The red markers indicate key peak positions calculated with DFT for the predicted layered hP8-LiB^{2D} phase.

cated by the presence of lower-symmetry structures (see Fig. 4). Second, the distortion of B chains takes the starting material part-way towards the new layered morphology. Fig. 1(e,f) illustrates how the B chains in oI8-LiB^{1D} can link into layers in hR12-LiB^{2D} without bond breaking. Hence, a transformation from LiB_y^{1D} to LiB^{2D} and $LiB_{y-\delta}^{1D}$ might take place before the layered material becomes thermodynamically stable. The kinetics of the full process involving local B rebonding and long-range Li redistribution is a challenge to simulate. However, the apparent ability of LiB_y^{1D} to change composition post-synthesis[17,24,26] and the evidence of successful rebonding in other covalent systems via cold compression[51] motivated us to attempt high-pressure synthesis under room-T conditions.

IV. HIGH-PRESSURE SYNTHESIS AND XRD CHARACTERIZATION

Our first goal was to investigate and rationalize the response of LiB_y^{1D} to high pressure. We predicted that the material's ground state composition(s) should shift towards the Li-rich end[17] and argued that the *change* in the interlayer Li-Li layer distance $c_{\text{Li-Li}}$ could be used to deduce the *variation* in stoichiometry (the typical 1-2% over- or underestimation of bond lengths in DFT presents a problem for pin-pointing the *absolute* composition)[17,24]. Another way to reduce the effect of systematic DFT errors in determining the LiB_y^{1D} stoichiometry is to monitor the $c_{\text{Li-Li}}/a_{\text{Li-Li}}$ ratio, as was done in recent studies[29,31]. The ratios obtained by fitting collected XRD patterns with hexagonal unit cells *decreased* with pressure[31] which was reasoned to result from the LiB_y^{1D} enrichment in Li[29].

Figs. 5-7 show evolution of reflections in compression-decompression runs. The best-resolved XRD patterns were obtained in samples immersed in oil while the pressure was changed from 6.5 GPa up to 33.2 GPa and back down to 3.5 GPa in Fig. 5. The presence of weak peaks (Fig. 5) from possible trace by-products of LiB_y^{1D} synthesis posed little problem in our XRD analysis of the key phases. In light of the established dynamical instability of hexagonal $Li_{2n}B_m^{1D}$ representative structures, it is surprising that the dominant peaks in the XRD patterns in previous[31] and present (Figs. 5-8) experiments could still be matched well to the (100), (10n), and (110) hexagonal lattice reflections. The sufficiently different XRD patterns for short-period phases (Fig. 4) were not detected in our experiments. The extracted and calculated $c_{\text{Li-Li}}/a_{\text{Li-Li}}$ ratios in Fig. 9 are consistent with the previous conclusion[29] that the compound's Li content increases above 6 GPa. In our case, the ratio changed by as much as $\Delta y \approx 3/4 - 9/10 = -0.15$ [$\Delta x \approx 0.04$ in Li_xB_{1-x} notation] once the pressure was raised to 30 GPa. The value agrees well with the previously calculated shift in the $H_{form}(x)$ parabolic minima by 0.04 by going from 0 to 30 GPa (Fig. 6 in Ref. 17).

The sets of data corresponding to pressure release give new insights into the behavior of compressed LiB_y^{1D}. First, the experimental $c_{\text{Li-Li}}/a_{\text{Li-Li}}$ ratios *decreased* and followed the calculated slopes once the pressure was dropped from the maximum values down to 20 GPa

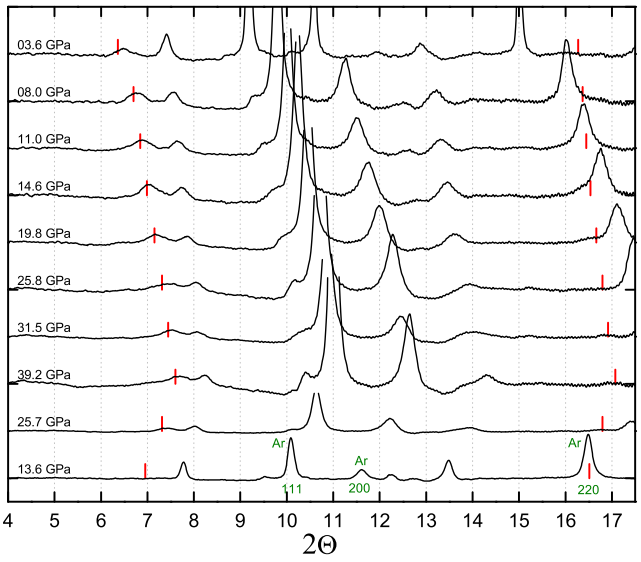

FIG. 7: (color online) Evolution of powder XRD peaks from LiB_y in the Ar pressure medium at room temperature and 13.6 → 39.2 → 3.6 GPa pressures. The red markers indicate key peak positions calculated with DFT for the predicted layered hP8-LiB_{2D} phase. The dominant peaks are from Ar.

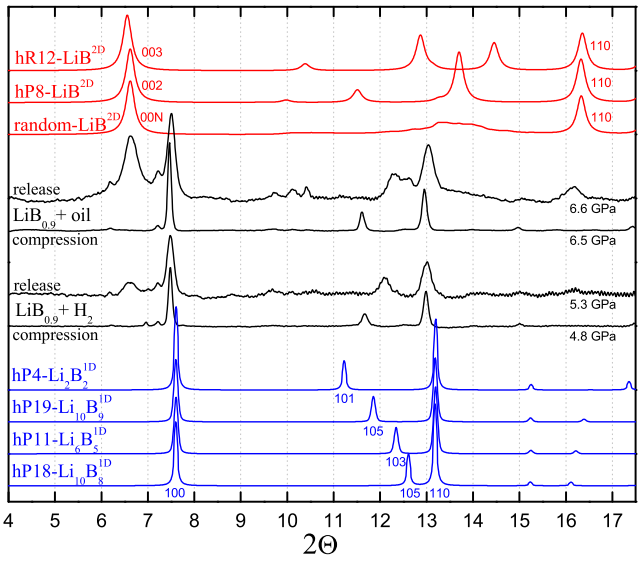

FIG. 8: (color online) The top three XRD patterns were simulated for predicted ordered/disordered phases with 2D B layers as explained in the text. The two sets of experimental patterns were collected before and after compression. The bottom four calculated patterns show how the intermediate (10n) peaks position could be used as a marker to determine $Li_{2n}B_m^{1D}$ composition. All simulation patterns were obtained at 6.5 GPa.

which suggests that the stoichiometry remained constant during that procedure. Second, the composition never returned to its starting value at about 6 GPa and differed by $\sim 0.02 \approx 6/11 - 10/19$. The "before and after" shots at similar $P \sim 6$ GPa in Fig. 8 illustrate an upshift of the intermediate (10n) peak by a considerable 0.5-0.6 degrees. The double peak around 12.5 degrees in the decompressed LiB_y+oil sample could be attributed to two co-existing LiB_y stoichiometries. In order to balance out the evident change in composition a different product must have had to form.

The most important XRD feature discovered in all our experiments was a strong peak appearing some 0.6 degree below the (100) LiB_y^{1D} reflection at 23/26/21 GPa in the oil/Ar/H_2 loadings and remaining visible down to 3.5 GPa in oil. Figs. 5-8 illustrate that the peak position is consistent with the calculated (002) reflection angle in hP8-LiB^{2D}. We had anticipated that because of the very small stacking fault energy in the predicted LiB^{2D} phase the reflection corresponding to the interlayer distance might be the only detectable signature[17]. Indeed, the intensity and width of peaks in structures with stacking faults depend on the degree (or presence) of long-range order[52]. Fig. 8 shows that the hR12 and hP8 structures with shortest stacking sequences have well-defined peaks in the 10-15 degree range. However, the LiB material with simulated random layer shifts (see SM[39] for details) has only a weak broad plateau in their place and could be responsible for the unusual sloped feature between 13.5 and 14.7 degrees in the collected 6.6 GPa pattern. The simulated (110) reflection should be visible in powder XRD and was indeed matched with the peak above 16 degrees (resolved best in the LiB_y^{1D}+oil sample) that appeared simultaneously with (002). The calculated structural parameters given for key phases in Tables S III-V[39] are within a typical 2% agreement with the ones extracted from the XRD data via LeBail fitting.

The evolution of the peak magnitudes was also in qualitative agreement with the described transformation of the starting material into its more Li-rich variant and the

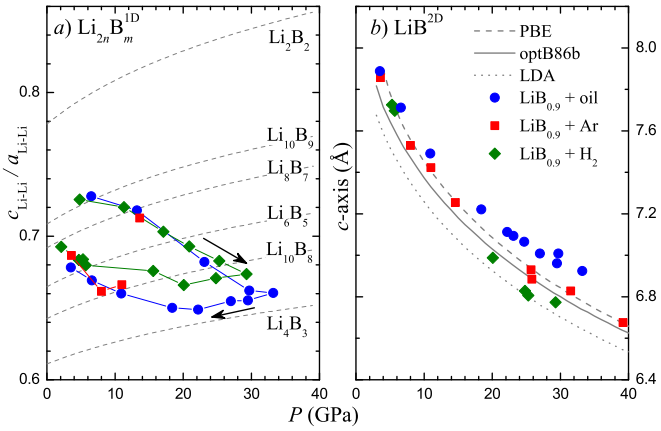

FIG. 9: (color online) (a) Ratios calculated with DFT (lines) are for $Li_{2n}B_m^{1D}$ structures with undistorted B chains; ratios extracted from the XRD data ($\lambda = 0.4422$ Å) were based on the (100), (10n), and (110) peak positions assuming the hexagonal structure (see Fig. 8). In LiB_y^{1D}+Ar reflections from Ar made it difficult to extract $c_{\text{Li-Li}}$ for $P > 15$ GPa. (b) Calculated and measured c-axis in the predicted hP8-LiB^{2D} phase based on the (002) peak.

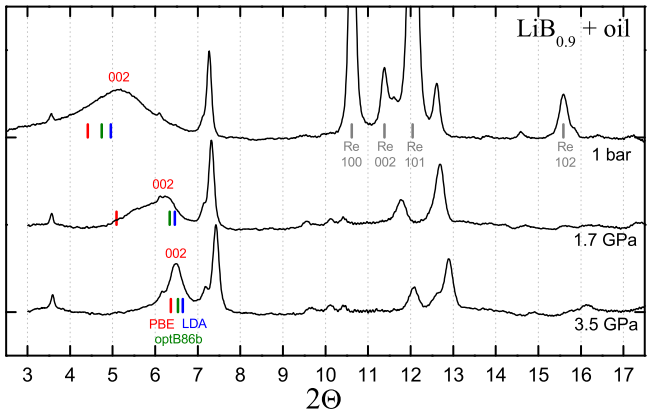

FIG. 10: (color online) XRD patterns for $LiB_{0.9}$ samples upon pressure release. The top pattern was observed for the DAC with the Re gasket as described in the text and Fig. S12. The bottom and middle patterns are the lowest-pressure points in the sequence shown in Fig. 5 obtained for the DAC with the Fe gasket. The grey bars mark reflections from hcp-Re. The red, olive, and blue bars indicate positions of the (002) LiB^{2D} reflection calculated with the GGA, optB86b, and LDA, respectively.

stoichiometric layered LiB^{2D}. The (002) peak in Figs. 5-7 was weak when it first appeared. It became comparable in magnitude to the neighbouring (100) peak at maximum pressures suggesting co-existence of roughly equal amounts of the remaining LiB_y^{1D} ($y \sim 0.8$) and the new LiB^{2D} phases. The (002) peak diminished upon decompression and could not be detected at 2.1 GPa in the loading with the H_2 pressure medium. The reflection could not be associated with any of the known phases in the oil/Ar/H_2 pressure media[39,53,54] or the Fe/Re gasket. The derived LiB_y^{1D} phases are clearly not responsible for the peak either, as the distortions cause an upshift of the dominant (100) peak and appearance of minor peaks at considerably larger angles (Fig. 4).

Remarkably, the (002) peak could still be detected at 1 bar in one loading as shown in Fig. 10. In that case, the XRD pattern was taken in the DAC with screws removed. The sample apparently shifted to the edge of the Re gasket and the hcp-Re peaks could be matched well with the known experimental ambient-pressure lattice constants: $a = 2.760$Å and $c = 4.458$Å. The considerable broadness of the peak is not a background feature as can be seen from the raw integrated signals in Fig. S12. For comparison, Fig. 10 also shows two lowest pressure XRD sets collected for the sample discussed in Fig. 5. The broadness of the peaks along with the large dispersion of the DFT values can be attributed to a dramatic change in the hP8-LiB^{2D} interlayer spacing in the 0-5 GPa range explained in Ref. 20 (any pressure gradient across the DAC and/or residual stress in the sample result in much larger peak widths in this case). The data indicate that the material can be quenched down to ambient pressure under certain conditions.

Achieving crystallization of phases with low stacking fault energies is a complicated and demanding process. In this case, subjecting the DAC's to moderate temperatures up to 100 C using a heat gun produced no significant changes in the XRD patterns. In the last set of exploratory experiments we laser-heated samples up to about 2,000 K. As Ar had been found to produce obstructing peaks and as we were also interested in the reaction of LiB_y with H_2, the experiments were carried out for the H_2 and oil pressure media. According to our preliminary analysis, multiple interesting reactions took place and we could identify only a subset of the products as known $LiBH_4$ and LiBC phases. Mapping the high-P phase diagram of Li-B and related systems will require further systematic study.

V. CONCLUSIONS

Our experimental and *ab initio* results reveal a remarkably complex behavior of the Li-B system at high pressures. Formation of the predicted layered LiB^{2D} material at *room* T above 21 GPa was not easy to detect and was evidenced by (i) the appearance of signature (002)/(110) peaks, expected to be strongest in the presence of stacking disorder; and (ii) the deduced increase in Li content of the starting LiB_y^{1D} material, needed to be balanced out via formation of a less Li-rich phase. It remains a puzzle why the (002) peak was not observed in the previous experiment[31] or why it was not detected up to 17 GPa in our case despite the evident change in the LiB_y^{1D} composition above 6 GPa.

Using DFT calculations we established that shortest-period $Li_{2n}B_m^{1D}$ representatives of the well-studied LiB_y^{1D} family become dynamically unstable quickly, above ~ 15 GPa. However, no distorted derivatives, such as the proposed stable mS14-$Li_4B_3^{1D}$ phase, were detected in the experiments and the obtained powder XRD patterns could still be fitted well with hexagonal unit cells. A scenario consistent with this observation would involve nucleation of the layered LiB^{2D} phase in the sample regions with buckled B chains while the excess Li is pushed into the remaining hexagonal matrix of LiB_y^{1D}.

According to our data in Fig. 10, the synthesized material is quenchable down to ambient pressure. Since the LiB_y^{1D} to LiB^{2D} transformation was observed just above 20 GPa, use of multi-anvil cells in future experiments should allow synthesis of the layered compound in sufficient quantities for further characterization and possible modification via doping. Probing its predicted superconducting properties should provide further insights into the importance of the different B states near the Fermi level on T_c[19–21] and help design new high-T_c MgB_2-type superconductors.

We thank A.K. Kleppe and N. Casati for help with setting up synchrotron measurements. A.N.K. and S.H. gratefully acknowledge the NSF support (Award No. 1410514).

[1] N. W. Ashcroft, Phys. Rev. Lett. **21**, 1748 (1968).
[2] J. Nagamatsu *et al.*, Nature (London) **410**, 63 (2001).
[3] H. Chena, T. N. Conga, W. Yanga, C. Tanb, Y. Lia, and Y. Ding, Progress in Natural Science **19**, 291 (2009).
[4] H. D. Yoo, E. Markevich, G. Salitra, D. Sharon, and D. Aurbach, Materialstoday **17**, 110 (2014).
[5] P. Jena, J. Phys. Chem. Lett. **2**, 206 (2011).
[6] A. Gurevich, Nat. Mater. **10**, 255 (2011).
[7] I. I. Mazin, Nature (London) **464**, 183 (2010).
[8] M. L. Cohen, J. Mater. Res. **26**, 2815 (2011).
[9] A. N. Kolmogorov, M. Calandra, S. Curtarolo, Phys. Rev. B **78**, 094520 (2008).
[10] K. J. Chang and M. L. Cohen, Phys. Rev. B **30**, 5376 (1984).
[11] J. B. Neaton and N. W. Ashcroft, Nature (London) **400**, 141 (1999).
[12] A. N. Kolmogorov, S. Shah, E. R. Margine, A. F. Bialon, T. Hammerschmidt, and R. Drautz, Phys. Rev. Lett. **105**, 217003 (2010).
[13] H. Gou *et al.*, Phys. Rev. Lett. **111**, 157002 (2013).
[14] A. P. Drozdov, M. I. Eremets, I. A. Troyan, V. Ksenofontov, and S. I. Shylin, Nature (London) **525**, 525, 73 (2015).
[15] D. Duan *et al.*, Sci. Rep. **4**, 6968 (2014).
[16] A. N. Kolmogorov and S. Curtarolo, Phys. Rev. B **73**, 180501(R) (2006).
[17] A. N. Kolmogorov and S. Curtarolo, Phys. Rev. B **74**, 224507 (2006).
[18] G. L. W. Hart, Nat. Mater. **6**, 941 (2007).
[19] A. Y. Liu and I. I. Mazin, Phys. Rev. B **75**, 064510 (2007).
[20] M. Calandra, A. N. Kolmogorov and S. Curtarolo, Phys. Rev. B **75**, 144506 (2007).
[21] E. Martinez-Guerra, F. Ortz-Chi, S. Curtarolo, and R. de Coss, J. Phys.: Condens. Matter **26**, 115701 (2014).
[22] H. Rosner, A. Kitaigorodsky, and W. E. Pickett, Phys. Rev. Lett. **88**, 127001 (2002).
[23] A. M. Fogg, J. B. Claridge, G. R. Darling, and M. J. Rosseinsky, Chem. Commun., 1348 (2003).
[24] A. N. Kolmogorov, R. Drautz, D. G. Pettifor, Phys. Rev. B **76**, 184102 (2007).
[25] M. Wörle and R. Nesper, Angew. Chem. **112**, 2439 (2000).
[26] M. Worle, R. Nesper, and T. K. Chatterji, Z. Anorg. Allg. Chem. **632** 1737 (2006).
[27] F. Peng, M. Miao, H. Wang, Q. Li, and Y. Ma, J. Am. Chem. Soc., **134**, 18599 (2012).
[28] A. Hermann, A. McSorley, N. W. Ashcroft, and R. Hoffmann, J. Am. Chem. Soc., **134**, 18606 (2012).
[29] A. Hermann, A. Suarez-Alcubilla, I. G. Gurtubay, L.-M. Yang, A. Bergara, N. W. Ashcroft, and R. Hoffmann, Phys. Rev. B **86**, 144110 (2012).
[30] A. G. Van Der Geest and A. N. Kolmogorov, CALPHAD **46**, 184 (2014).
[31] A. Lazicki, R. J. Hemley, W. E. Pickett, and Choong-Shik Yoo, Phys. Rev. B **82**, 180102(R) (2010).
[32] G. Kresse and J. Hafner, Phys. Rev. B **47**, 558 (1993); G. Kresse and J. Furthmüller, Phys. Rev. B **54**, 11169 (1996).
[33] J. D. Pack and H. J. Monkhorst, Phys. Rev. B **13**, 5188 (1976); **16**, 1748 (1977).
[34] P.E. Blöchl, Phys. Rev. B **50**, 17953 (1994).
[35] J. P. Perdew, K. Burke, and M. Ernzerhof, Phys. Rev. Lett. **77**, 3865 (1996).
[36] J.P. Perdew, K. Burke, and M. Ernzerhof, Phys. Rev. Lett. **78**, 1396 (1997).
[37] J.P. Perdew, and A. Zunger, Phys. Rev. B **23**, 5048 (1981).
[38] J. Klime, D.R. Bowler, and A. Michaelides, J. Phys.: Condens. Matter **22**, 022201 (2010).
[39] See EPAPS Document No. 1.
[40] D. Alfè, Comp. Phys. Commun. **180**, 2622 (2009).
[41] A. N. Kolmogorov, http:\\maise-guide.org
[42] G. Bruzzone, J. Less-Common Met. **25**, 361 (1971).
[43] A. N. Kolmogorov, S. Shah, E. R. Margine, A. K. Kleppe, and A. P. Jephcoat, Phys. Rev. Lett. **109**, 075501 (2012).
[44] A.P. Hammersley, ESRF Internal Report, **ESRF97HA02T** (1997).
[45] A.P. Hammersley, S.O. Svensson, M. Hanfland, A.N. Fitch, and D. Hüsermann, High Pressure Research **14**, 235-248 (1996).
[46] A. Coelho, TOPAS-ACADEMIC, version 4.1, Coelho Software, Brisbane (2007).
[47] H. Rosner and W. E. Pickett, Phys. Rev. B **67**, 054104 (2003).
[48] A. Suarez-Alcubilla, I. G. Gurtubay, and A. Bergara, J. Phys.: Condens. Matter **26**, 475402 (2014).
[49] A. Togo, and I. Tanaka, Phys. Lett. B **87**, 184104 (2013).
[50] S. Shah and A. N. Kolmogorov, Phys. Rev. B **88**, 014107 (2013).
[51] W. L. Mao *et al.*, Science **302**, 425 (2003).
[52] T. Kogure, J. Kameda, T. Matsui, and R. Miyawakiz, Am. Mineral. **91**, 1363 (2006).
[53] J. W. Otto, J. K. Vassiliou, and G. Frommeyer, Phys. Rev. B **57**, 3253 (1998).
[54] A.P. Jephcoat and S.P. Besedin, in *Properties of Earth and Planetary materials at High Pressure and temperature*, Geophys. Monogr. **101**, edited by M.H. Manghnani and T. Yagi (American Geophysical Union, 1998), pp. 287-296.